IEEE Open Journal of
Power Electronics

Received 15 October 2022; revised 5 December 2022; accepted 13 December 2022. Date of publication 19 December 2022;
date of current version 30 December 2022. The review of this article was arranged by Associate Editor Zedong Zheng.

Digital Object Identifier 10.1109/OJPEL.2022.3230399

Efficiency-Oriented Parameter Design and Comparison of Medium Voltage Isolated Bidirectional DC/DC Converters

RUNTIAN CHEN [1] (Student Member, IEEE), RUI LU [1] (Student Member, IEEE), XIANZHE BAO [1] (Student Member, IEEE), CHUSHAN LI [1,2] (Member, IEEE), WUHUA LI [1] (Member, IEEE), AND XIANGNING HE [1] (Fellow, IEEE)

[1]College of Electrical Engineering, Zhejiang University, Hangzhou 310027, China
[2]Zhejiang University–University of Illinois at Urbana Champaign Institute, Zhejiang University, Haining 314400, China

CORRESPONDING AUTHOR: CHUSHAN LI (e-mail: lichushan@hotmail.com.)

This work was supported by the National Natural Science Foundation of China under Grants U1834205, 51925702, and 52061635101.
This paper is an extension of a conference paper "Advanced Parameter Optimization Strategy and Quantitative Evaluation of the Isolated Bidirectional Resonant DC-DC Converter," in 2021 IEEE 12th Energy Conversion Congress & Exposition - Asia (ECCE-Asia), which was held on May 24th–27th in Singapore.

ABSTRACT In a medium voltage (MV) solid state transformer(SST), the isolated bidirectional DC/DC converter (IBDC) is the core circuit for controlling power flow and galvanic isolation. Current research works on MV single-cell IBDC mainly focus on two directions: resonant and non-resonant topologies. However, for different scenarios with various voltage regulation ranges and power ranges, which topology should be adopted to achieve better efficiency performance is unclear. To effectively illustrate the two IBDCs' respective benefits, a comparison between the two IBDCs is conducted in this study along with the optimization design method. For resonant IBDC, a complex objective optimization-based parameter design strategy is developed to realize rapid automatic design under various operating conditions. For non-resonant IBDC, a multi-phase modulation scheme aimed at minimizing the current stress under different voltage and power ranges is introduced. The optimal operating range of the two IBDCs has been derived. A 4 kV/1 kV 200 kW non-resonant IBDC experimental prototype has been built and its efficiency is tested under various operating conditions. The test data were compared with the established power loss model to derive the converter's full range efficiency, and the efficiency of the converter over a wider power range could then be projected.

INDEX TERMS DC/DC converters, dual active bridge (DAB), resonant converters, design methodology, medium voltage (MV), solid state transformer (SST).

I. INTRODUCTION

A large number of new energy power generation equipment and new power consumption equipment connected to the power grid make it difficult for the traditional AC system to maintain the economic operation range and guarantee the stability of the power grid operation. Therefore, the AC/DC hybrid system that can meet these requirements has become the future construction direction [1]. Many AC/DC hybrid system demonstration projects have been carried out successively, such as the IGREENGrid project [2] and the IDE4L project [3] of the EU, the CLASS project [4] of the U.K. and the FICS project [5] of the US.

In AC/DC hybrid system, solid state transformer (SST) is the core equipment, also known as power electronic transformer (PET), which generally refers to the novel power electronic equipment using power electronic technology and medium and high frequency transformer technology. Specifically, SST is widely used in various energy conversion applications such as data center power supply, traction system, energy network interconnection, electric vehicle charging, and so forth [6], [7], [8]. High transmission power, high power density, and high efficiency are typically required for these applications. The isolated bidirectional DC/DC converter (IBDC) is the power electronic interface between a

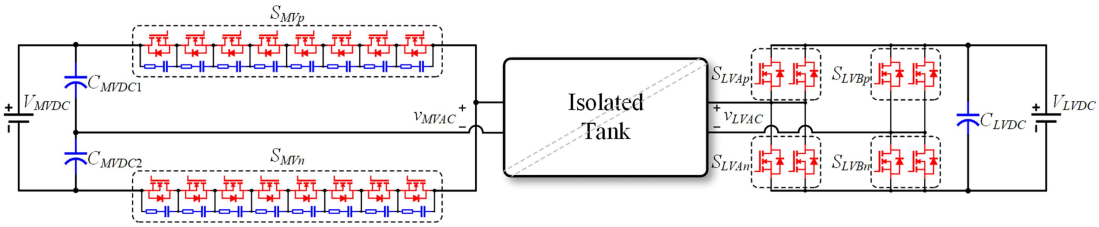

FIGURE 1. The structure of the evaluated IBDC.

medium voltage (MV) bus and a low voltage (LV) bus and acts as the most crucial part of the SST, which undertakes many functions such as galvanic isolation, power control and voltage gain regulation. The loss of IBDC accounts for a large proportion of the overall loss of SST [9] and the IBDC with single-cell structure has an advantage in efficiency due to its simple structure and less number of components.

The rapid development of MV power devices makes the single-cell structure of IBDC possible. A few prototypes have been created currently. A 6 kV 10 kW IBDC based on 15 kV SiC MOSFET has been developed and its peak efficiency exceeds 98% [10]. Besides, A 7 kV 25 kW IBDC based on 10 kV SiC MOSFET has been realized which achieves an unprecedented power density of 3.28 kW/L [11]. However, it could be predicted that there will not be commercial or widely available MV power devices in the next five years, and there is an urgent need for a solution that could replace MV power devices.

For the reasons listed above, the equivalent construction of MV power devices by connecting LV power devices in series and its applications in IBDC have attracted much attention. In two series-connected device examples with 10 kV/10 A SiC MOSFET and 15 kV/20 A SiC IGBT on the HV side, [12] evaluates a 16 kV/1 MW DC-DC building block. Besides, a design example of the 99% efficient 5 kV 30 kW experimental prototype is presented which combines the soft switching characteristics of the converter and series-connected devices' voltage sharing properties [13]. The IBDC to be designed in this paper will be based on the power electronics building block (PEBB) set up in [14], and its voltage balancing is mainly realized by applying RC snubber circuit and controlling the gate drive delay. After sufficient design and experimental verification, the maximum voltage imbalance could be limited under 10% of the average voltage on each device with 150A switching current. The structure of the evaluated IBDC is shown in Fig. 1. In this structure, a symmetrical half bridge composed of series-connected SiC MOSFETs is set on the MV side, a full bridge composed of parallel-connected SiC MOSFETs is arranged on the LV side, and both sides are connected by isolated tank.

According to the configuration of the isolated tank and the modulation method, the IBDC can be roughly classified into two types: isolated bidirectional resonant DC/DC converter (IBRDC) and isolated bidirectional non-resonant DC/DC converter (IBNDC) [15], as shown in Fig. 2. In general, IBRDC's

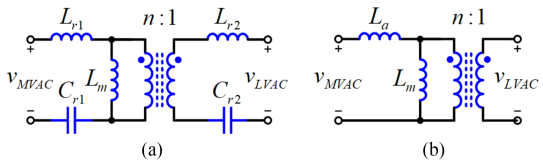

FIGURE 2. Different types of isolated tank. (a) Isolated tank in IBRDC. (a) Isolated tank in IBNDC.

voltage regulation range is relatively narrow, but it can realize a full range of soft switching. In most cases, IBRDC adjusts the voltage gain by frequency modulation. On the contrary, the voltage regulation range of IBNDC is relatively wide, while the soft switching state is limited by certain conditions. IBNDC typically modifies the voltage gain by combining pulse width modulation and phase shift modulation. The above experience-based knowledge can provide guidance for topology selection of IBDC in many occasions, but there is still a problem that the quantitative boundary of these two IBDCs optimal application scenarios is not clear. To address this issue, this study compares the two converters' best operating ranges based on optimal parameter design and specify the converter construction strategy.

The analysis of the IBRDC involves the selection of multiple resonant components. To further clarify the relationships among the resonant components, several parameters are used [16], [17], [18], [19]. Because of their interdependence, these factors cannot be developed separately. Every parameter may need to be modified in response to changes in other parameters. In the design optimization of IBRDC, particle swarm optimization is used to design parameters with high system stability and 50% duty cycle open-loop control [20]. However, the design process is not intuitive enough to make the development process very complicated. From another perspective, an accurate description of the gain characteristics and resonant behaviors by analyzing operation mode are provided, and then an optimal design methodology have been proposed [21]. While in [22], the IBRDC is designed by adopting the statistical design of the experiment based on asymmetric parameters methodology. However, they still rely on trial and error for the design process. The labor-intensive method cannot be employed for quantitative analysis, necessitating the development of an autonomous optimization procedure. In addition, because some algorithms oversimplify the resonant

TABLE 1. Design Targets of the Evaluated IBDC

Target	Value
Rated Power P_{rat}	200 kW
Rated Medium DC Voltage $V_{MVDCrat}$	4 kV
Rated Low DC Voltage $V_{LVDCrat}$	1 kV
Snubber Capacitor on MV Side C_s	4.7 nF
Snubber Resistor on MV Side R_s	5 Ω
Power Device on MV Side	BSM180D12P2E002 (8-Series)
Power Device on LV Side	BSM250D17P2E004 (2-Parallel)

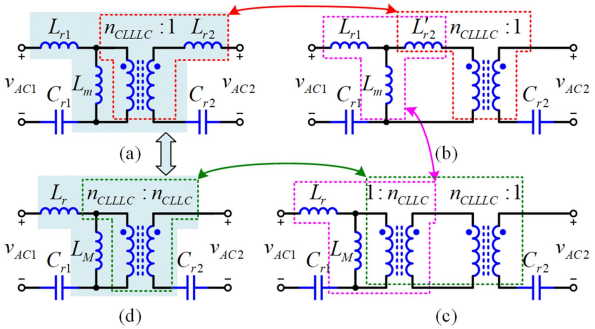

FIGURE 3. Equivalent process of the two main types of resonant tank in IBRDC. (a) CLLLC type resonant tank. (b) Equivalent process of the secondary side resonant inductance. (c) Equivalent process from T-type network to Γ-type network. (d) CLLC type resonant tank.

parameters, the types of resonant parameters considered still need to be further supplemented.

Design targets of the evaluated IBDC are shown in Table 1. The rest of the paper is organized as follows. Section II proposes the automatic parameter optimization strategy of IBRDC. The modulation scheme and parameter design are described in Section III. The efficiency analysis and comparison of these two IBDCs are illustrated in Section IV. The construction of the prototype and experimental verification are presented in Section V. Finally, Section VI concludes this article.

II. PARAMETER OPTIMIZATION STRATEGY OF IBRDC

A. DEFINITIONS AND ASSUMPTIONS

There are two main types of the resonant tank in the high-power application scenarios: CLLLC type and CLLC type. However, these two types of resonant tank are essentially the same [23], and can be equivalent in terms of parameters through the process shown in Fig. 3. The parameter relationship of the equivalent process is shown in (1). Therefore, the following design work is based on the CLLLC type.

$$\begin{cases} n_{CLLC} = (n^2 L_{r2} + L_m)/L_m \\ L_M = L_m^2/(n^2 L_{r2} + L_m) \\ L_r = L_{r1} + L_m - L_M \end{cases}. \tag{1}$$

In the designed IBRDC, the forward state is defined as a state in which energy is transmitted from the primary side to the secondary side in a single switching period, while the reverse state is the opposite. Additionally, Pulse Frequency Modulation (PFM) is adopted for the source side bridge arm

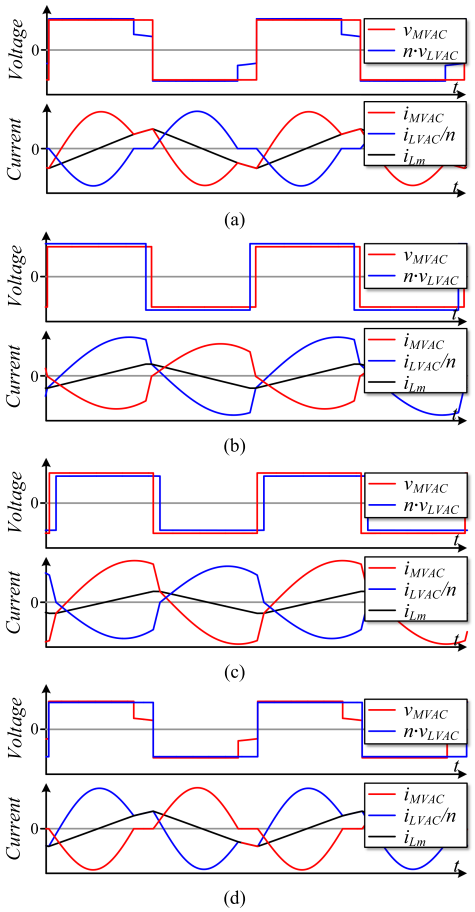

FIGURE 4. Main waveforms of IBRDC with PFM. (a) $v_{MVDC}<2n.v_{LVDC}$ in forward state. (b) $v_{MVDC}<2n.v_{LVDC}$ in reverse state. (c) $v_{MVDC}\geq 2n.v_{LVDC}$ in forward state. (d) $v_{MVDC}\geq 2n.v_{LVDC}$ in reverse state.

and uncontrolled rectification is adopted for the load side bridge arm. Main waveforms of IBRDC with PFM are shown in Fig. 4. As shown in the figure, the switching frequency of the active bridges on the source side should decrease with the increase of gain. When IBRDC operates in the forward state with $v_{MVDC}<2n.v_{LVDC}$ or in the reverse state with $v_{MVDC}\geq 2n.v_{LVDC}$, the active bridges on the source side could achieve zero voltage switching (ZVS) and the rectifier bridges on the load side would operate in zero current switching (ZCS) mode. While in other states, the active bridges could still achieve ZVS, but the ZCS mode of the rectifier bridges on the load side would be lost.

There are multiple resonant elements in the resonant tank, these resonant elements are coupled with each other, which is not conducive to parameter design. The definition of these two resonant frequencies and the ratios between the resonant elements are shown in (2).

$$\begin{cases} g = C'_{r2}/C_{r1} \\ h = L'_{r2}/L_{r1} \\ \omega_1 = 1/\sqrt{L_{r1}C_{r1}} \\ \omega_2 = 1/\sqrt{L_{r2}C_{r2}} \end{cases}. \tag{2}$$

Therefore, it is necessary to unify two resonant frequencies into one resonant frequency with $g{\cdot}h{=}1$ [24]. As a result, the resonant parameter relationship in this case is defined as shown in

$$\begin{cases} g = C'_{r2}/C_{r1} = L_{r1}/L'_{r2} \\ k = L_m/L_{r1} \\ Q_{for} = \sqrt{L_{r1}/C_{r1}}/R_{for} \end{cases}. \tag{3}$$

where R_{for} denotes the equivalent AC load resistance of the forward state, and Q_{for} is the equivalent MV side quality factor of the series resonant circuit formed by L_{r1}, C_{r1} and R_{for} in forward state.

B. OPTIMIZATION TARGET AND CONSTRAINTS

The automatic parameter design process is developed based on optimization target and constraints. The resonant current should be kept to a minimum in order to minimize the ohmic losses of the resonant tank as well as the switching and conduction losses of power devices. Thus, it is important to increase the input impedance. The input impedance might be maximized by increasing the magnetic inductance as much as feasible because the total reactance of the series resonant tank is zero at the resonant frequency. So the optimization target is to maximize the product of k and Q_{for}, as shown in

$$\left|Z_{infor}\right| = \frac{1}{\sqrt{1+\frac{1}{k^2 Q_{for}^2}}} R_{for}. \tag{4}$$

The constraints of the IBRDC design can be divided into five categories: maximum gain, derivative of gain, inductive input impedance, switching current and maximum capacitor voltage. The reasons and formulas for setting various constraints have been given specifically in [24].

C. AUTOMATIC PARAMETER DESIGN

Based on the optimization target and constraints described above, an automatic design process for resonant parameters applicable to the IBRDC is developed, as shown in Fig. 5. First, three parameters k, g, and Q_{for} are defined according to the external requirements of the designed converter. With the target of maximizing the product of k and Q_{for}, parameters are constrained to be calculated in terms of maximum gain, derivative of gain, inductive input impedance, switching current, and maximum capacitor voltage. Then, n groups of initial arrays are specified to avoid the optimization result from falling into the local optimal solution. These initial arrays are solved using the Ipopt local optimization solver and the Pyomo nonlinear programming tool, and the resulting optimized parameter arrays are verified on the PLECS simulation platform. The optimized resonant parameters are output if the loss obtained from the simulation is less than 1% change from the previous one.

D. PARAMETER OPTIMIZATION RESULTS ANALYSIS

The regulation range of DC bus voltage will have a great impact on the IBRDC's parameters, and then affect the efficiency

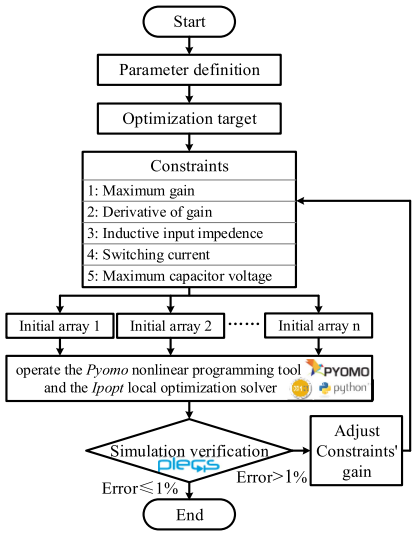

FIGURE 5. Automatic parameter design process.

of the converter. In order to indicate the regulation range of DC bus voltage, two parameters are defined, as shown in

$$\begin{cases} \alpha_{MV} = \left(V_{MVDCmax} - V_{MVDCmin}\right)/V_{MVDCrat} \\ \alpha_{LV} = \left(V_{LVDCmax} - V_{LVDCmin}\right)/V_{LVDCrat} \end{cases}. \tag{5}$$

The optimization results are displayed in Fig. 6, where the red and purple dots represent the curves' terminal points and the red and purple stars represent the curves' diverging points. It can be summarized in the following aspects.

1) k declines, but Q_{for} and g rise with α_{MV} when the resonant capacitor voltage constraint is not considered.
2) With the limitation of capacitor voltage $V_{Cr1max}{=}\ 0.5V_{MVDCmin}$ and $V_{Cr2max}{=}\ V_{LVDCmin}$, the trend of resonant parameters changes. When α_{MV} is less than the value indicated by the red star, the changes in the resonant parameters are identical to those when the capacitor voltage restriction is ignored, as demonstrated in Fig. 6(a)~(c). The falling rate of k becomes slow when α_{MV} exceeds the value associated with the red star, while Q_{for} and g no longer increase but instead steadily decline.
3) As α_{LV} is adjusted, the changes of k and Q_{for} are the same as those of α_{MV}, but the trend in g is altered. As α_{LV} increases, g decreases. When the capacitor voltage limit is applied, g would turn up at the purple and red stars and would end at the purple and red dots.

In conclusion, it can be seen that the voltage regulation range and the maximum voltage limitation of the resonant capacitor have a significant impact on the trend of resonant parameters. Specifically, when the voltage regulation range is rather wide, the resonant capacitor voltage limitation would affect the resonant parameters. This influence will cause the optimization target, or the product of k and Q_{for}, to fall. This would further increase the resonant current. This section also provides a reference for the engineering design of the IBRDC by describing the trend of each resonant parameter.

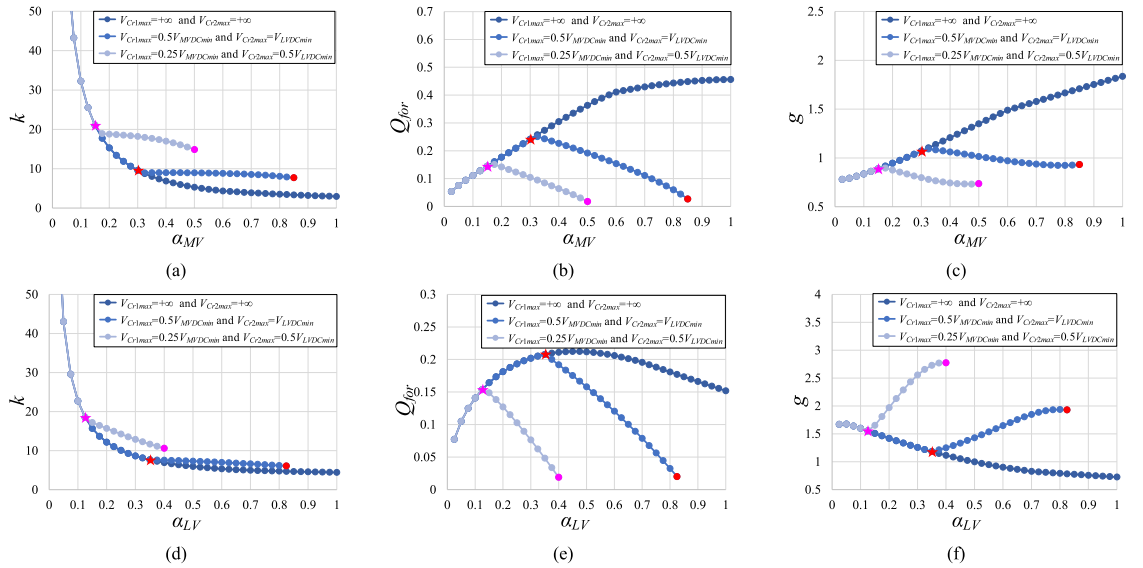

FIGURE 6. Variation of optimized resonant parameters with voltage regulation range. (a) The influence of α_{MV} on k. (b) The influence of α_{MV} on Q_{for}. (c) The influence of α_{MV} on g. (d) The influence of α_{LV} on k. (e) The influence of α_{LV} on Q_{for}. (f) The influence of α_{LV} on g.

III. MODULATION AND PARAMETER DESIGN OF IBNDC

The isolated tank of the IBNDC is composed of an auxiliary inductor and a transformer, wherein the value of the auxiliary inductor could be expressed as

$$L_a = \frac{nV_{MVDCmin}V_{LVDCmin}}{4f_s\frac{P_{rat}}{\eta_{total}}}(\varphi_{Cmax}(1-\varphi_{Cmax})). \quad (6)$$

If φ_{Cmax} is set to 1/2, it corresponds to the upper limit of the transmission power. However, the linear relationship between φ_C and transmission power is weak and the effective value of the isolated tank current would be large in this case. So it is not conducive to improving the efficiency. On the other hand, φ_{Cmax} cannot be too small, which requires high control accuracy. After comprehensive consideration, φ_{Cmax} =1/4 is set in this paper.

In the modulation aspect, the duty ratio of the half bridge drive on the MV side is fixed to 0.5, and the phase shift between the arms of the full bridge drive on the low-voltage side is controlled to minimize the circulating power in the converter. Therefore, according to the waveform relationship of the primary and secondary side voltage of the transformer, the modes of the converter are divided into four types, as shown in Fig. 7(a). In the figure, φ_C is defined as the phase shift angle duty ratio of the rising edge of the positive level between the primary and secondary side voltages, and φ_I is the duty ratio of the non-zero level of the secondary side AC voltage. After each mode's isolated tank current has been examined, the mode with the lowest peak value of isolated tank current under the same transmission power is chosen to run. Fig. 7(b) shows the mode selection strategy, where $M = 2nV_{LVDC}/V_{MVDC}$ and p is the normalized transmission power which could be expressed as $p = P/P_{max}$. B_0 mode and D_0 mode are special cases of B mode and D mode when $\varphi_I = 0.5$. The expressions of control variables under each mode

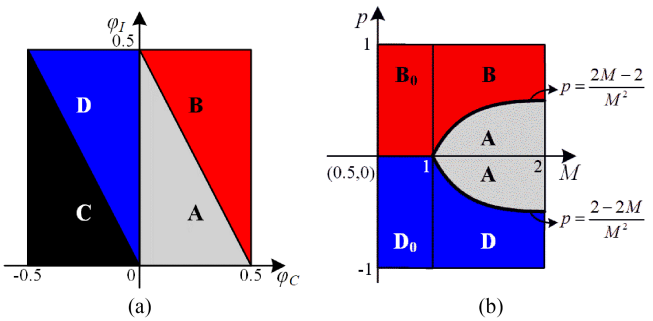

FIGURE 7. Modes of IBNDC. (a) Modes definition. (b) Mode selection strategy according to M and p.

TABLE 2. Control Variable Expression in Each Mode

Mode	φ_I	φ_C
A	$\frac{1}{4}(1+\sqrt{1-2\lvert p\rvert})$	$\frac{1}{4}(1-\sqrt{1-\lvert p\rvert})$
B	$\frac{1}{2}+\frac{1}{2}(1-M)\sqrt{\frac{1-p}{2-2M+M^2}}$	$\frac{1}{4}(2-2\varphi_I-\sqrt{4\varphi_I-4\varphi_I^2-p})$
D	$\frac{1}{2}+\frac{1}{2}(1-M)\sqrt{\frac{1+p}{2-2M+M^2}}$	$\frac{1}{4}(-2\varphi_I+\sqrt{4\varphi_I-4\varphi_I^2+p})$

are shown in Table 2. Main waveforms of IBNDC with the multi-phase-shift modulation scheme are shown in Fig. 8. In the figure, five different modes are presented respectively.

Theoretically, the auxiliary inductor has a great influence on the magnitude of the current flowing on it. If the voltage regulation range is wide, that is, $V_{MVDCmin}$ and $V_{LVDCmin}$ are relatively low, the auxiliary inductor would be small. In order to quantitatively analyze the prediction, the primary and secondary sides should select different voltage regulation

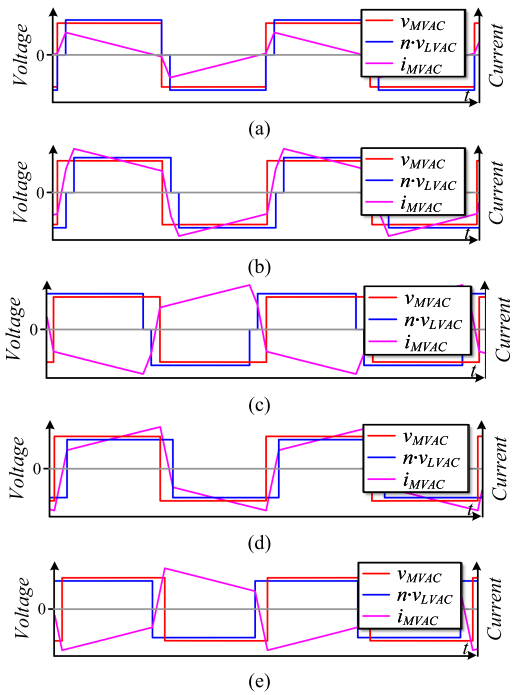

FIGURE 8. Main waveforms of IBNDC with multi-phase-shift modulation scheme. (a) Mode A. (b) Mode B. (c) Mode D. (d) Mode B_0. (e) Mode D_0.

ranges for comparison. In the voltage regulation range compared, different voltage ratios on both sides are selected for efficiency analysis.

IV. EFFICIENCY COMPARISON OF IBDCS

According to the operation state of the two IBDCs in a single switching period, the conduction current and the switching current of the devices on both sides can be calculated. With the characteristics of the devices, the conduction loss and switching loss of the devices on both sides can be obtained. The power device loss models of the two IBDCs are systematically built in MathCAD, and a simulation model based on PLECS platform has been used to confirm the accuracy of the loss calculation model. Subsequently, the efficiency of the converter's power device would be evaluated using a MathCAD loss calculation model to accelerate the evaluation process.

The losses in the forward and reverse states are not the same, so these two cases need to be considered separately. This is mainly because different resonant elements are used when the IBRDC operates in different states, and power devices on both sides are different. According to Table 1, eight 1200V SiC MOSFETs (BSM180D12P2E002) are connected in series on the MV side, four 1700V SiC MOSFETs (BSM250D17P2E004) are used parallelly on the LV side. Therefore, all evaluations in this section consider the influence of forward and reverse states on power device loss. In order to explore the influence of the maximum DC voltage regulation range on the loss of the converter, while fixing the DC voltage on one side, this section adopts the previously defined α_{MV} and α_{LV} measure the maximum variation range of bus voltage on both sides of the converter. Within a certain maximum DC voltage regulation range, the power device efficiency corresponding to different DC voltages under the same load rate is averaged to obtain the average power device efficiency curve within the range.

Fig. 9(a) shows the change of the average power device efficiency with α_{MV} in the forward state. With the expansion of the voltage regulation range, the power device efficiency gradually decreases, and the downward trend of IBRDC is more obvious. When $\alpha_{MV} \leq 0.10$, the average power device efficiency of IBRDC is higher, and when $\alpha_{MV} > 0.10$, the average power device efficiency of the IBNDC is higher. Especially when $\alpha_{MV} > 0.25$, the average power device efficiency of IBRDC is very low, which cannot meet the operation requirements of the converter. Fig. 9(b) shows the average efficiency of the converter with α_{MV} in the reverse state. It is similar to that in the forward state, but due to different device characteristics and components in resonance, the reverse device efficiency of IBRDC decreases to some extent. In some extreme states, because the magnetic inductance of the IBRDC is too small and the circulating power in the isolated tank is too large, the IBNDC occupies an absolute advantage.

Fig. 10(a) shows the change of the average power device efficiency with α_{LV} in the forward state, and Fig. 10(b) shows that in the reverse state. Compared with α_{MV}, α_{LV} has less influence on IBRDC. And when α_{LV} is relatively large, the power device efficiency of IBRDC is still lower than that of IBNDC.

In conclusion, α_{MV} and α_{LV} have approximately the same effect on the average power device efficiency of the converter. The power device efficiency decreases with the increase of the maximum regulation range of DC voltages. When $\alpha_{MV} \leq 0.10$ or $\alpha_{LV} \leq 0.10$, IBRDC should be adopted, while IBNDC is more suitable for $\alpha_{MV} > 0.10$ or $\alpha_{LV} > 0.10$.

V. EXPERIMENTAL VERIFICATION

According to the above analysis, when the voltage regulation rate is 0.5, IBNDC has an absolute efficiency advantage over IBRDC. Therefore, IBNDC will be deveolped as the target in this section.

A. KEY PARAMETER DESIGN

In order to facilitate the modular design, two 1:1 transformers are connected in primary-series-secondary- parallel pattern, equivalently forming a 2:1 transformer. Under full load, the operating condition of $V_{MVDC} = 4000$ V and $V_{LVDC} = 750$ V is the operating condition with the maximum effective value of current and the theoretical loss. In this working condition, the apparent power of a single transformer is about 150 kVA. Based on (6) and Table 1, it can be determined that the total auxiliary inductance seen from the primary side is 70 μH. Circuit configuration of the isolated tank is shown in Fig. 11. In the figure, total auxiliary inductance consists of transformer leakage inductance L_{kT} and external auxiliary inductance L_{aEx}. The external auxiliary inductor is made into

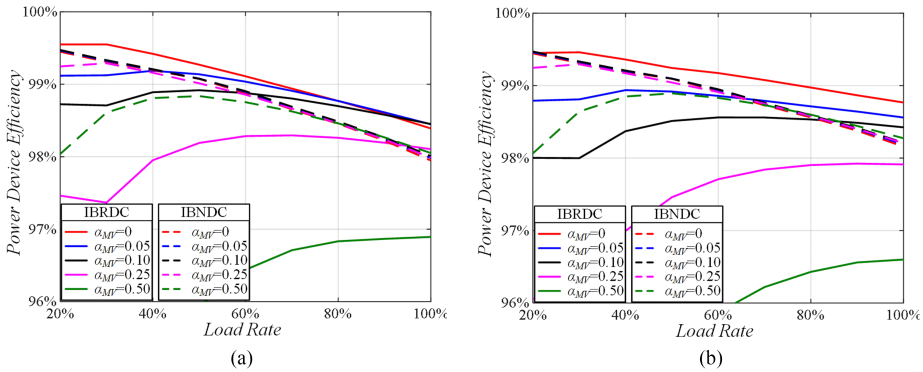

FIGURE 9. Influence of MV DC voltage regulation range on power device efficiency of IBDC. (a) Power device efficiency in forward state. (b) Power device efficiency in reverse state.

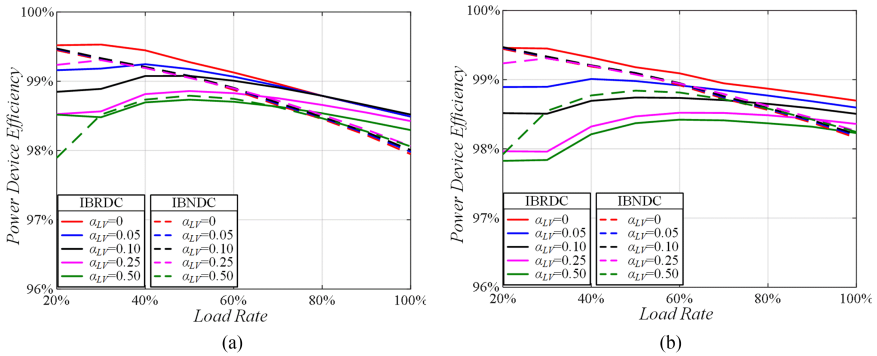

FIGURE 10. Influence of LV DC voltage regulation range on power device efficiency of IBDC. (a) Power device efficiency in forward state. (b) Power device efficiency in reverse state.

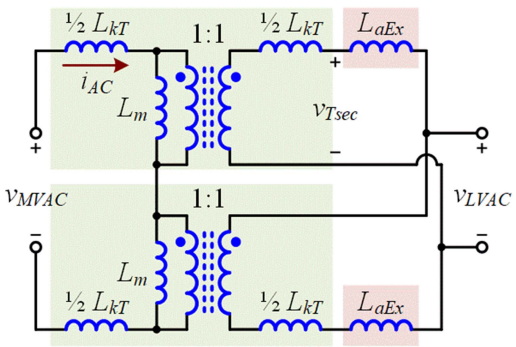

FIGURE 11. Circuit configuration of isolated tank in IBNDC.

discrete components to effectively reduce the heat dissipation pressure and reduce the isolation requirements of the high voltage across the inductors, which is also conducive to the arrangement in space.

The maximum voltage ripple of half bridge capacitor is set as 1.5% of the 1/2 V_{MVDC}. Limited by the voltage and current requirements of a single capacitor, the two capacitors are connected in parallel and then three groups are connected in series to obtain a capacitance of 80 μF that can guarantee a maximum ripple of 1.46% on the MV side. The maximum voltage ripple of V_{LVDC} is also set to 1.5%. The two capacitors are connected in series and then four groups are connected in parallel to obtain a capacitance of 136 μF which can ensure a maximum ripple of 1.47% on the LV side. To sum up, the parameters of the developed IBNDC is shown in Table 3.

TABLE 3. Parameters of the Developed IBNDC

Parameter	Value
Apparent Power of a Single Transformer S_{Trat}	150kVA
Transformer Leakage Inductance L_{kT}	17μH
External Auxiliary Inductance L_{aEx}	18μH
MV DC Capacitance C_{MVDC1}/C_{MVDC2}	80μF
LV DC Capacitance C_{LVDC}	136μF

B. CONSTRUCTION OF EXPERIMENTAL PROTOTYPE

In addition to power isolation by transformer, the IBNDC developed in this paper also needs to realize the isolation of the control system and the auxiliary power supply system, so as to realize the full isolation of the MV and LV sides. In MV applications, magnetic coupling and optical transmission are generally used to achieve isolation.

In this paper, the auxiliary power supply is realized by multi-stage magnetic coupling. The signal interaction between the MV side and the LV side is realized through optical transmission. In view of these considerations, the control system structure with isolation between MV side and LV side could be shown as Fig. 12. The MV control board and the

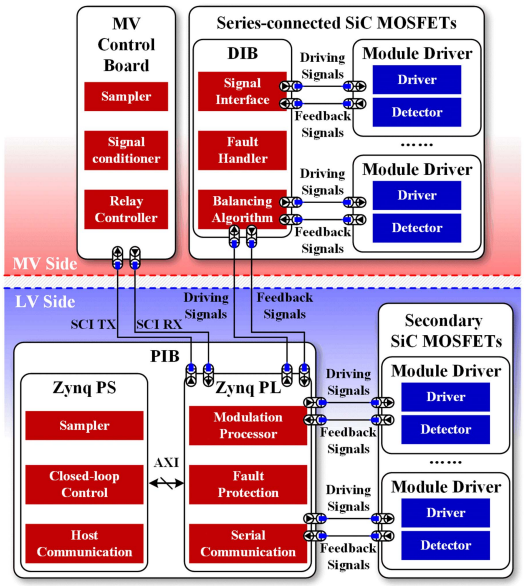

FIGURE 12. Control system structure with isolation between MV side and LV side.

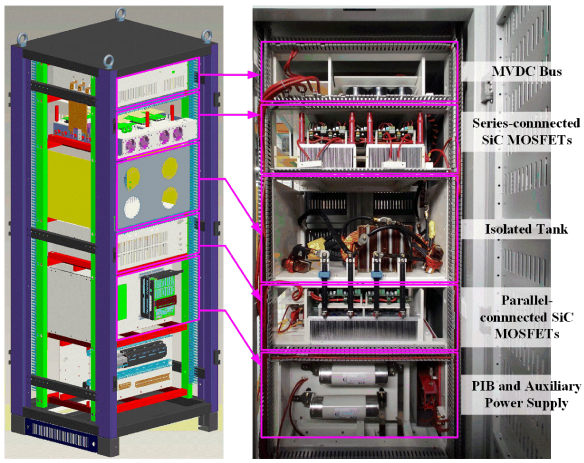

FIGURE 13. Converter's assembly drawing and experimental prototype.

power interface board (PIB) realize the interaction of control signals and sampling data on the optical fiber through serial communication interface (SCI). The module driver on the LV side and the distribution interface board (DIB) on the MV side are connected to the PIB through optical fibers to transmit driving signals and feedback signals.

The converter has been assembled layer by layer from top to bottom in the order of MV to LV. The converter's assembly drawing and experimental prototype are presented in Fig. 13. The highest layer is equipped with MV DC bus capacitors, corresponding sensing circuits and MV control board. The series-connected SiC MOSFETs are set in the second highest layer. The middle layer is equipped with transformers and external auxiliary inductors. The next layer includes parallel-connected SiC MOSFETs, LV DC bus capacitors and corresponding sensing circuits. PIB, auxiliary power supply,

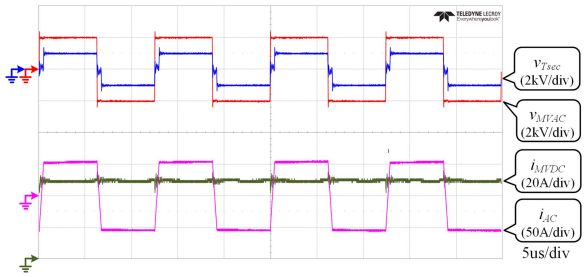

FIGURE 14. Main waveforms in 4 kV/1 kV experiment with 100 kW load.

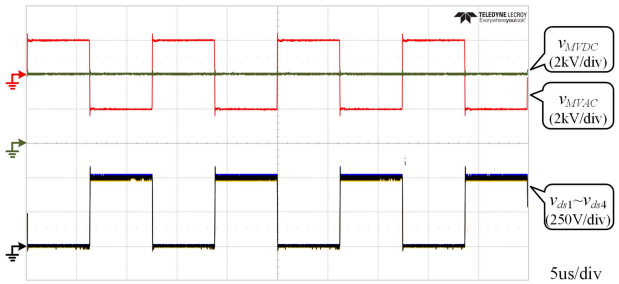

FIGURE 15. MV DC bus waveform and voltage sharing among SiC MOSFETs.

discharging circuits and protection circuits are arranged at the lowest layer.

C. MV HIGH POWER EXPERIMENT

In order to verify the MV high power operating capacity of the designed IBNDC, 4000V/1000V 100kW experiment is carried out, and the main waveforms are shown in Fig. 14. The experimental waveforms are close to the simulation results. The primary side voltage of the isolated tank is switched between ± 2 kV. The voltage v_{Tsec} shown in Fig. 11 is switched between ± 1 kV and near zero voltage level. This is because the overall leakage inductance of the transformer is close to the external auxiliary inductance, v_{Tsec} is near zero when the voltage across the overall auxiliary inductance is clamped by the superposed voltage at both ends of the isolated tank. The AC current measured at the primary side of the transformer is trapezoidal, and its maximum value exceeds 50 A.

In addition, the MV DC bus waveform and voltage sharing among SiC MOSFETs has been observed in Fig. 15. Under the tested conditions, the voltage ripple of the MV DC bus is less than 1%. Under the support of synchronous gate drive delay correction technology, the maximum voltage difference among SiC MOSFETs is less than 5%. To sum up, the above experiments prove the functional integrity of the designed IBDC, which pave the way for further expanding the application of IBDC in the MV high power field.

Finally, the efficiency under half load with different DC bus voltages was measured, as shown in Fig. 16. Limited by the peripheral experimental conditions, the maximum power tested at present can only reach half load, but the relevant measurements are sufficient for correcting the loss model coefficients for each part of the converter. The loss model

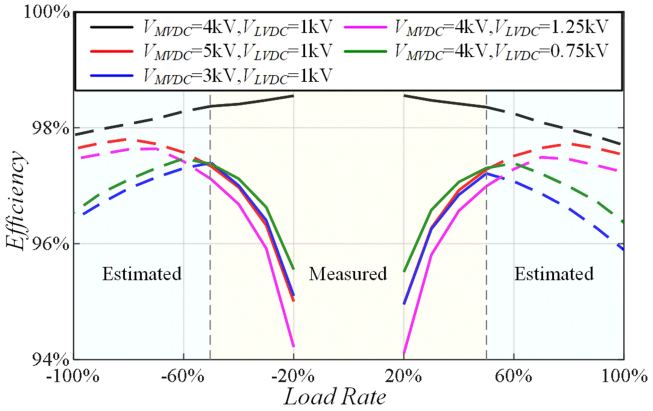

FIGURE 16. The measured and estimated efficiency of the designed converter with different DC bus voltages.

includes the switching loss and conduction loss of the power devices on both sides, the losses of the magnetic components, and the losses of capacitors and power line. Among them, since the loss data of the devices are obtained by double-pulse experiment, the switching and conduction losses are similar to the predicted results, and no correction is required. The magnetic element losses could be divided into core losses and winding losses, and the equivalent loss model have been verified by simulation and corrected by correction coefficients. The losses of capacitors and power line could be obtained from the datasheet based on the classical calculation model, accounting for a small proportion. This part of the losses is not corrected in the model and has little impact on the overall loss model. The loss model is used to predict the converter efficiency when the load is greater than half load, as shown by the dashed line in the figure. The experimental results show that the converter can operate efficiently. When the primary side matches secondary side, the efficiency can reach 98% at half load. Even when the primary and secondary sides do not match, the efficiency can still exceed 97% at half load.

VI. CONCLUSION

In this paper, an MV IBDC based on series-connected SiC MOSFETs has been proposed. Firstly, the structure of the MV IBDC is presented which is the basis for the comparison between IBRDC and IBNDC. Subsequently, an automatic parameter optimization strategy for IBRDC is proposed and an optimal modulation strategy for IBNDC is introduced. The optimal operating range of the two IBDC in terms of voltage regulation range and load rate is then studied from the perspective of power device efficiency. Then IBNDC is selected as the topology of the developed converter. Considering the galvanic isolation of power circuit and control circuit, a 4 kV/1 kV 200 kW experimental prototype has been set up. The experiments carried out can prove the functional integrity and MV high power transmission capability of the converter. At last, the measured and estimated efficiency of the designed converter with different DC bus voltages is presented to prove the high efficiency operation capability.

REFERENCES

[1] F. Nejabatkhah and Y. W. Li, "Overview of power management strategies of hybrid AC/DC microgrid," *IEEE Trans. Power Electron.*, vol. 30, no. 12, pp. 7072–7089, Dec. 2015.
[2] J. Varela, N. Hatziargyriou, L. J. Puglisi, M. Rossi, A. Abart, and B. Bletterie, "The IGREENGrid project: Increasing hosting capacity in distribution grids," *IEEE Power Energy Mag.*, vol. 15, no. 3, pp. 30–40, May/Jun. 2017.
[3] S. Repo et al., "The IDE4L project: Defining, designing, and demonstrating the ideal grid for all," *IEEE Power Energy Mag.*, vol. 15, no. 3, pp. 41–51, May/Jun. 2017.
[4] A. Ballanti, L. N. Ochoa, K. Bailey, and S. Cox, "Unlocking new sources of flexibility: Class: The world's largest voltage-led load-management project," *IEEE Power Energy Mag.*, vol. 15, no. 3, pp. 52–63, May/Jun. 2017.
[5] B. Currie et al., "Flexibility is key in New York: New tools and operational solutions for managing distributed energy resources," *IEEE Power Energy Mag.*, vol. 15, no. 3, pp. 20–29, May/Jun. 2017.
[6] S. A. Saleh et al., "Solid-state transformers for distribution systems–Part II: Deployment challenges," *IEEE Trans. Ind. Appl.*, vol. 55, no. 6, pp. 5708–5716, Nov./Dec. 2019.
[7] J. E. Huber and J. W. Kolar, "Applicability of solid-state transformers in today's and future distribution grids," *IEEE Trans. Smart Grid*, vol. 10, no. 1, pp. 317–326, Jan. 2019.
[8] M. A. Hannan et al., "State of the art of solid-state transformers: Advanced topologies, implementation issues, recent progress and improvements," *IEEE Access*, vol. 8, pp. 19113–19132, 2020.
[9] D. Rothmund, G. Ortiz, T. Guillod, and J. W. Kolar, "10 kV SiC-based isolated DC-DC converter for medium voltage-connected solid-state transformers," in *Proc. IEEE Appl. Power Electron. Conf. Expo.*, 2015, pp. 1096–1103.
[10] L. Wang, Q. Zhu, W. Yu, and A. Q. Huang, "A medium-voltage medium-frequency isolated DC–DC converter based on 15-kV SiC MOSFETs," *IEEE J. Emerg. Sel. Topics Power Electron.*, vol. 5, no. 1, pp. 100–109, Mar. 2017.
[11] D. Rothmund, T. Guillod, D. Bortis, and J. W. Kolar, "99.1% efficient 10 kV SiC-based medium-voltage ZVS bidirectional single-phase PFC AC/DC stage," *IEEE J. Emerg. Sel. Topics Power Electron.*, vol. 7, no. 2, pp. 779–797, Jun. 2019.
[12] K. Vechalapu, A. K. Kadavelugu, and S. Bhattacharya, "High voltage dual active bridge with series connected high voltage silicon carbide (SiC) devices," in *Proc. IEEE Energy Convers. Congr. Expo.*, 2014, pp. 2057–2064.
[13] Z. Lu et al., "Medium voltage soft-switching DC/DC converter with series-connected SiC MOSFETs," *IEEE Trans. Power Electron.*, vol. 36, no. 2, pp. 1451–1462, Feb. 2021.
[14] C. Li et al., "Analytical model and design of voltage balancing parameters of series-connected SiC MOSFETs considering non-flat miller plateau of gate voltage," *Energies*, vol. 15, Feb. 2022, Art. no. 1722.
[15] B. Zhao, Q. Song, W. Liu, and Y. Sun, "Overview of dual-active-bridge isolated bidirectional DC–DC converter for high-frequency-link power-conversion system," *IEEE Trans. Power Electron.*, vol. 29, no. 8, pp. 4091–4106, Aug. 2014.
[16] J.-H. Jung, H.-S. Kim, M.-H. Ryu, and J.-W. Baek, "Design methodology of bidirectional CLLC resonant converter for high-frequency isolation of DC distribution systems," *IEEE Trans. Power Electron.*, vol. 28, no. 4, pp. 1741–1755, Apr. 2013.
[17] X. Li, J. Huang, Y. Ma, X. Wang, J. Yang, and X. Wu, "Unified modeling, analysis, and design of isolated bidirectional CLLC resonant DC–DC converters," *IEEE J. Emerg. Sel. Top. Power Electron.*, vol. 10, no. 2, pp. 2305–2318, Apr. 2022.
[18] J. Min and M. Ordonez, "Bidirectional resonant CLLC charger for wide battery voltage range: Asymmetric parameters methodology," *IEEE Trans. Power Electron.*, vol. 36, no. 6, pp. 6662–6673, Jun. 2021.
[19] P. He, A. Mallik, A. Sankar, and A. Khaligh, "Design of a 1-MHz high-efficiency high-power-density bidirectional GaN-based CLLC converter for electric vehicles," *IEEE Trans. Veh. Technol.*, vol. 68, no. 1, pp. 213–223, Jan. 2019.

[20] F. Lin, X. Zhang, and X. Li, "Design methodology for symmetric CLLC resonant DC transformer considering voltage conversion ratio, system stability, and efficiency," *IEEE Trans. Power Electron.*, vol. 36, no. 9, pp. 10157–10170, Sep. 2021.
[21] Z. Lv, X. Yan, Y. Fang, and L. Sun, "Mode analysis and optimum design of bidirectional CLLC resonant converter for high-frequency isolation of DC distribution systems," in *Proc. IEEE Energy Convers. Congr. Expo.*, 2015, pp. 1513–1520.
[22] J. Min and M. Ordonez, "Asymmetric parameters design for bidirectional resonant CLLC battery charger," in *Proc. IEEE Energy Convers. Congr. Expo.*, 2020, pp. 5375–5379.
[23] Z. U. Zahid, Z. M. Dalala, R. Chen, B. Chen, and J.-S. Lai, "Design of bidirectional DC–DC resonant converter for vehicle-to-grid (V2G) applications," *IEEE Trans. Transp. Electrific.*, vol. 1, no. 3, pp. 232–244, Oct. 2015.
[24] R. Chen et al., "Advanced parameter optimization strategy and quantitative evaluation of the isolated bidirectional resonant DC-DC converter," in *Proc. IEEE 12th Energy Convers. Congr. Expo.-Asia*, 2021, pp. 562–567.

RUNTIAN CHEN (Student Member, IEEE) received the B.S. degree in electrical engineering from the School of Electrical Engineering and Automation, Harbin Institute of Technology, Harbin, China, in 2018. He is currently working toward the Ph.D. degree in electrical engineering with the College of Electrical Engineering, Zhejiang University, Hangzhou, China. His research interests include series-connected SiC power MOSFETs and their applications in high power medium voltage converters.

RUI LU (Student Member, IEEE) was born in Liaoning, China. He received the B.S. degree in electrical engineering from the College of Electrical Engineering, Zhejiang University, Hangzhou, China, in 2018. He is currently working toward the Ph.D. degree in electrical engineering with the Zhejiang University–University of Illinois at Urbana-Champaign Institute, Zhejiang, China. His research interests include modeling and design of medium-voltage high-frequency magnetic components, and high power converters.

XIANZHE BAO (Student Member, IEEE) received the B.E.E. degree from the Hubei University of Technology, Wuhan, China, in 2021. He is currently working toward the Ph.D. degree with Zhejiang University, Hangzhou, China. His research interests include high voltage series-connected IGBTs and IGBT modeling technology.

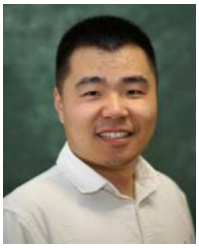

CHUSHAN LI (Member, IEEE) received the B.E.E. and Ph.D. degrees in electrical engineering from the Department of Electrical Engineering, Zhejiang University, Hangzhou, China, in 2008 and 2014, respectively. He is currently an Assistant Professor with the Zhejiang University – University of Illinois at Urbana-Champaign Institute, Zhejiang, China. From April to September in 2008, he was an Internship Student with the Power Application Design Center, National Semiconductor (Hong Kong) Co.Ltd. From December 2010 to October 2011, he was a Visiting Scholar with Freedm Center, North Carolina State University, Raleigh, NC, USA. From December 2013 to June 2014, he was a Research Assistant with The Hong Kong Polytechnic University, Hong Kong. From July 2014 to July 2017, he was a Postdoctoral Fellow with the Department of Electrical and Computer Engineering, Ryerson University, Toronto, ON, Canada. His research interests include high power density power converter design and transportation electrification.

WUHUA LI (Member, IEEE) received the B.Sc. and Ph.D. degrees in power electronics and electrical engineering from Zhejiang University, Hangzhou, China, in 2002 and 2008, respectively.

From 2004 to 2005, he was a Research Intern, and from 2007 to 2008, a Research Assistant with GE Global Research Center, Shanghai, China. From 2008 to 2010, he joined the College of Electrical Engineering, Zhejiang University as a Post doctor. In 2010, he was promoted as an Associate Professor. Since 2013, he has been a Full Professor with Zhejiang University. From 2010 to 2011, he was a Ryerson University Postdoctoral Fellow with the Department of Electrical and Computer Engineering, Ryerson University, Toronto, ON, Canada. He is currently the Executive Deputy Director of the National Specialty Laboratory for Power Electronics and the Vice Director of the Power Electronics Research Institute, Zhejiang University. He has authored or coauthored more than 300 peer-reviewed technical papers and holds more than 50 issued/pending patents. His research interests include power devices, converter topologies, and advanced controls for high power energy conversion systems.

Due to his excellent teaching and research contributions, he was the recipient of the 2012 Delta Young Scholar from Delta Environmental & Educational Foundation, 2012 Outstanding Young Scholar from National Science Foundation of China (NSFC), 2013 Chief Youth Scientist of National 973 Program, 2014 Young Top-Notch Scholar of National Ten Thousand Talent Program, and 2019 Distinguished Young Scholar from National Science Foundation of China. He is an Associated Editor for the *Journal of Emerging and Selected Topics in Power Electronics*, *IET Power Electronics*, *CSEE Journal of Power and Energy Systems*, *CPSS Transactions on Power Electronics and Applications*, *Proceedings of the Chinese Society for Electrical Engineering*, the Guest Editor of *IET Renewable Power Generation* for Special Issue DC and HVDC system technologies, a Member of the Editorial Board of the *Journal of Modern Power System and Clean Energy*.

He was the recipient of one National Natural Science Award and four Scientific and Technological Achievement Awards from Zhejiang Provincial Government and the State Educational Ministry of China. Since 2014, he has been the Most Cited Chinese Researcher by Elsevier.

XIANGNING HE (Fellow, IEEE) received the B.Sc. and M.Sc. degrees from the Nanjing University of Aeronautical and Astronautical, Nanjing, China, in 1982 and 1985, respectively, and the Ph.D. degree from Zhejiang University, Hangzhou, China, in 1989.

From 1985 to 1986, he was an Assistant Engineer with the 608 Institute of Aeronautical Industrial General Company, Zhuzhou, China. From 1989 to 1991, he was a Lecturer with Zhejiang University. In 1991, he obtained a Fellowship from the Royal Society of U.K., and conducted research with the Department of Computing and Electrical Engineering, Heriot-Watt University, Edinburgh, U.K., as a Postdoctoral Research Fellow for two years. In 1994, he joined Zhejiang University as an Associate Professor. Since 1996, he has been a Full Professor with the College of Electrical Engineering, Zhejiang University. He was the Director of the Power Electronics Research Institute, Head of the Department of Applied Electronics, Vice Dean of the College of Electrical Engineering, and is currently the Director of the National Specialty Laboratory for Power Electronics, Zhejiang University. His research interests include power electronics and their industrial applications.

Dr. He was appointed as IEEE Distinguished Lecturer by the IEEE Power Electronics Society during 2011–2015. He is also a Fellow of the Institution of Engineering and Technology (formerly IEE), U.K.